

PROBING THE GASEOUS DISK OF T Tau N WITH CN 5–4 LINES

L. PODIO^{1,2}, I. KAMP³, C. CODELLA¹, B. NISINI⁴, G. ARESU⁵, S. BRITAIN⁶, S. CABRIT^{2,7},
C. DOUGADOS^{2,8}, C. GRADY^{9,10}, R. MEIJERINK^{3,11}, G. SANDELL¹², M. SPAANS³,
W.-F. THI², G. J. WHITE^{13,14}, AND P. WOITKE¹⁵

¹ INAF-Osservatorio Astrofisico di Arcetri, Largo E. Fermi 5, I-50125, Florence, Italy

² UJF-Grenoble 1/CNRS-INSU, Institut de Planétologie et d’Astrophysique de Grenoble (IPAG) UMR 5274, Grenoble, F-38041, France

³ Kapteyn Astronomical Institute, University of Groningen, Landleven 12, 9747 AD Groningen, The Netherlands

⁴ INAF-Osservatorio Astronomico di Roma, via di Frascati 33, I-00040, Monte Porzio Catone, Italy

⁵ INAF-Osservatorio Astronomico di Cagliari, Via della Scienza 5, I-09047, Selargius, Italy

⁶ Department of Physics & Astronomy, 118 Kinard Laboratory, Clemson University, Clemson, SC 29634, USA

⁷ LERMA, Observatoire de Paris, UMR 8112 CNRS/INSU, 61 Av. de l’Observatoire, F-75014, Paris, France

⁸ LFCA, UMI 3386, CNRS and Dept. de Astronomia, Universidad de Chile, Santiago, Chile

⁹ Eureka Scientific, 2452 Delmer, Suite 100, Oakland, CA 96002, USA

¹⁰ Exoplanets & Stellar Astrophysics Laboratory, NASA Goddard Space Flight Center, Code 667, Greenbelt, MD 20771, USA

¹¹ Leiden Observatory, Leiden University, P.O. Box, NL-2300 RA Leiden, The Netherlands

¹² SOFIA-USRA, NASA Ames Research Center, MS 232-12, Building N232, Rm. 146, P.O. Box 1, Moffett Field, CA 94035-0001, USA

¹³ Department of Physical Sciences, The Open University, Milton Keynes, MK7 6AA, UK

¹⁴ RALSpace, The Rutherford Appleton Laboratory, Chilton, Didcot, OX11 0QX, UK

¹⁵ SUPA, School of Physics and Astronomy, University of St. Andrews, KY16 9SS, UK

Received 2014 January 7; accepted 2014 January 27; published 2014 February 24

ABSTRACT

We present spectrally resolved observations of the young multiple system T Tau in atomic and molecular lines obtained with the Heterodyne Instrument for the Far Infrared on board *Herschel*. While CO, H₂O, [C II], and SO lines trace the envelope and the outflowing gas up to velocities of 33 km s⁻¹ with respect to systemic, the CN 5–4 hyperfine structure lines at 566.7, 566.9 GHz show a narrow double-peaked profile centered at systemic velocity, consistent with an origin in the outer region of the compact disk of T Tau N. Disk modeling of the T Tau N disk with the thermo-chemical code ProDiMo produces CN line fluxes and profiles consistent with the observed ones and constrain the size of the gaseous disk ($R_{\text{out}} = 110_{-20}^{+10}$ AU) and its inclination ($i = 25^\circ \pm 5^\circ$). The model indicates that the CN lines originate in a disk upper layer at 40–110 AU from the star, which is irradiated by the stellar UV field and heated up to temperatures of 50–700 K. With respect to previously observed CN 2–1 millimeter lines, the CN 5–4 lines appear to be less affected by envelope emission, due to their larger critical density and excitation temperature. Hence, high- J CN lines are a unique confusion-free tracer of embedded disks, such as the disk of T Tau N.

Key words: astrochemistry – ISM: molecules – protoplanetary disks – stars: individual (T Tau)

Online-only material: color figures

1. INTRODUCTION

The study of the physical and chemical structure of protoplanetary disks is crucial to comprehend the formation of planetary systems. According to models, disks have a stratified structure, and hence different molecular species probe the physical and chemical conditions of different layers from the warm irradiated surface down to the cold midplane. Disks around non-embedded T Tauri and Herbig stars have been imaged in CO (e.g., Dutrey et al. 1998; Qi et al. 2004; Piétu et al. 2007), and detected in a number of other millimeter (mm) and submillimeter molecular lines (e.g., Dutrey et al. 1997; Thi et al. 2004). On the contrary, the study of disks around more embedded systems is obstructed by the associated envelopes and outflows which also emit strongly in the same molecular lines, hiding the fainter disk emission.

Recent studies show that CN is a good disk tracer with 88% of the T Tauri disks detected in CO 2–1 which are also observed in the CN 2–1 lines (Öberg et al. 2010, 2011; Chapillon et al. 2012). Moreover, Guilloteau et al. (2013) performed an IRAM 30-m survey of T Tauri and Herbig Ae systems located mainly in the Taurus-Auriga region and show that the CN 2–1 lines are less affected by the emission from the surrounding molecular cloud than the lines from CO isotopologues. However, CN 2–1

lines are still dominated by envelope/outflow emission in the case of actively accreting/ejecting sources, such as T Tau.

T Tau is a multiple system driving at least two bipolar jets detected in optical, near-infrared forbidden lines (Bohm & Solf 1994; Eisloffel & Mundt 1998; Solf & Böhm 1999; Herbst et al. 2007). The system consists of the northern component T Tau N ($M_* = 2.1 M_\odot$) and of the binary system T Tau Sa+Sb located 0'7 to the south ($M_* = 2.1, 0.8 M_\odot$, separation Sa–Sb = 0'13; Köhler et al. 2008). T Tau N is optically visible and is surrounded by an almost face-on, intermediate mass disk ($i < 30^\circ$, $M_{\text{disk}} \sim 0.01 M_\odot$) and an optically thin envelope (Beckwith et al. 1990; Hogerheijde et al. 1997; Akeson et al. 1998; Ratzka et al. 2009; Guilloteau et al. 2011). Both southern components, instead, are strongly obscured ($A_V \simeq 15, 30$ mag toward T Tau Sb and Sa, respectively), possibly due to a circumbinary envelope and, for T Tau Sa, to its almost edge-on disk ($i \sim 72^\circ$; Duchêne et al. 2005; Ratzka et al. 2009). Sa and Sb are not detected at mm wavelengths suggesting that their disks are small and of low-mass ($M_{\text{disk}} \sim 10^{-5} - 10^{-3} M_\odot$, $R_{\text{out}} \sim 5$ AU; Hogerheijde et al. 1997; Ratzka et al. 2009). While the dusty disk of T Tau N has been mapped in the mm, there are only very tentative observations of its gaseous disk, e.g., in the H₂ near-infrared lines (Gustafsson et al. 2008). Emission in the [O I]63 μm , [C II]157 μm , and [Ne II]12.81 μm lines is extended

Table 1
Observed Lines

Transition	ν_0^a (GHz)	E_{up} (K)	HPBW ($''$)	T_{peak} (mK)	V_{peak} (km s $^{-1}$)	ΔV (km s $^{-1}$)	$\int T_{mb}dV$ (K km s $^{-1}$)	F_{obs} (W m $^{-2}$)	F_{mod} (W m $^{-2}$)
CN 5–4 9/2–7/2	566.731	82	37	21/25 \pm 6 ^b	6.7/9.1 \pm 0.5 ^b	7	0.08 \pm 0.01	5.4 \pm 0.6 10 $^{-19}$	5.7 10 $^{-19}$
CN 5–4 11/2–9/2	566.947	82	37	25/28 \pm 6 ^b	6.3/8.4 \pm 0.5 ^b	7	0.12 \pm 0.01	8.1 \pm 0.6 10 $^{-19}$	6.7 10 $^{-19}$
o-H $_2$ O 1 $_{10}$ –1 $_{01}$	556.936	61	38	682 \pm 6	8.6 \pm 0.5	52	5.40 \pm 0.02	3.70 \pm 0.02 10 $^{-17}$	3.5 10 $^{-19}$
p-H $_2$ O 1 $_{11}$ –0 $_{00}$	1113.343	53	19	873 \pm 8	8.6 \pm 0.3	52	9.85 \pm 0.02	1.344 \pm 0.003 10 $^{-16}$	2.2 10 $^{-18}$
o-H $_2$ O 3 $_{12}$ –2 $_{21}$	1153.127	249	18	900 \pm 75	6.2 \pm 0.3	21	7.2 \pm 0.1	1.02 \pm 0.02 10 $^{-16}$	6.9 10 $^{-19}$
CO 10–9	1151.985	304	18	13210 \pm 75	7.7 \pm 0.3	38	82.9 \pm 0.2	1.171 \pm 0.002 10 $^{-15}$	1.4 10 $^{-17}$
13 CO 10–9	1101.350	291	19	1248 \pm 8	7.7 \pm 0.3	20	4.92 \pm 0.01	6.64 \pm 0.02 10 $^{-17}$	3.1 10 $^{-18}$
SO 12 $_{13}$ –11 $_{12}$	558.087	194	38	19 \pm 6	7.2 \pm 0.5	9	0.08 \pm 0.01	5.3 \pm 0.7 10 $^{-19}$	7.5 10 $^{-20}$
[C II] $^2P_{3/2}$ – $^2P_{1/2}$	1900.537	91	11	1120 \pm 83	7.1 \pm 0.2	30	8.4 \pm 0.1	1.95 \pm 0.03 10 $^{-16}$	4.8 10 $^{-17}$

Notes.

^a Frequencies are from the Jet Propulsion Laboratory database (JPL; Pickett et al. 1998) and from the Cologne Database of Molecular Spectroscopy (CDMS; Müller et al. 2001) for CN.

^b For the double-peaked CN lines the intensity and velocity of both peaks is reported.

and/or velocity-shifted, and hence likely associated with outflowing gas, while molecular lines, such as high- J CO, OH, and H $_2$ O lines, are spectrally and spatially unresolved (Spinoglio et al. 2000; van Boekel et al. 2009; Podio et al. 2012). Observations of low- J CO lines (Edwards & Snell 1982; Schuster et al. 1993) as well as of less abundant molecular species, such as 13 CO, C 17 O, o-H $_2$ CO, SO, and CN 2–1 are also dominated by envelope/outflow emission, preventing us to trace the gas in the disk (Guilloteau et al. 2013).

In this Letter, we present observations of the T Tau system in atomic and molecular lines with higher excitation energies than probed by Guilloteau et al. (2013) in the mm range obtained with the Heterodyne Instrument for the Far Infrared (HIFI) on board *Herschel*. While CO, 13 CO, H $_2$ O, [C II], and SO lines are still strongly dominated by emission from the surrounding envelope and outflows, the CN 5–4 lines allow digging out the faint emission from the disk of T Tau N.

2. OBSERVATIONS AND DATA REDUCTION

We observed T Tau ($\alpha_{J2000} = 04^h21^m59^s.4$, $\delta_{J2000} = +19^\circ32'06''.4$) with the HIFI (de Graauw et al. 2010) on board the *Herschel Space Observatory*¹⁶ (Pilbratt et al. 2010). The observations target the two fundamental water lines, o-H $_2$ O 1 $_{10}$ –1 $_{01}$ and p-H $_2$ O 1 $_{11}$ –0 $_{00}$ in the HIFI bands 1 and 4, the 12 CO (hereafter CO) 10–9 line in band 5, and the [C II] $^2P_{3/2}$ – $^2P_{1/2}$ line in band 7 (OBSID: 1342249419, 1342250207, 1342249598, 1342249647). They were acquired with a single on-source pointing and in dual beam switch mode with fast chopping 3' either side of the target. The achieved rms noise in bands 1, 4, 5, 7 is of 6, 8, 75, 83 mK, respectively. The Wide Band Spectrometer (WBS) and the High Resolution Spectrometer were used in parallel, providing a spectral resolution of 1.10 and 0.25 MHz, respectively. The half power beam width (HPBW) ranges from $\sim 11''$ to $\sim 38''$, depending on frequency. Hence, all the three sources of the T Tau system (N, Sa, and Sb) are covered by the observations. The selected spectral settings also cover with the WBS the CN 5–4 $J = 9/2$ – $7/2$ and $J = 11/2$ – $9/2$, SO 12 $_{13}$ –11 $_{12}$, 13 CO 10–9, and o-H $_2$ O 3 $_{12}$ –2 $_{21}$ lines.

The HIFI data were reduced using HIPE 10.¹⁷ Fits files from level 2 were then created and transformed into GILDAS¹⁸ format for data analysis. The spectra were baseline subtracted and averaged over the horizontal and vertical polarization to increase the signal-to-noise ratio. Antenna temperatures, T_a , were converted to mean beam temperature, T_{mb} , using mean beam efficiency by Roelfsema et al. (2012).

The properties of the detected lines (transition, frequency, ν_0 , upper level energy, E_{up}), the HPBW, and the measured parameters (peak temperature and velocity, T_{peak} and V_{peak} , the full line width at 1σ rms noise, ΔV , integrated intensity, $\int T_{mb}dV$, and line fluxes, F_{obs} ¹⁹) are summarized in Table 1.

3. RESULTS FROM OBSERVATIONS

The detected lines in Figure 1 show a variety of profiles indicating that they probe different gas components in the complex T Tau system.

The CO and 13 CO 10–9 lines show a single-peaked profile, likely dominated by cloud emission, and red-shifted and blue-shifted wings with velocities up to -8 and $+30$ km s $^{-1}$ probing outflowing gas. Assuming an average local interstellar medium (ISM) carbon isotope ratio of 68 ± 15 (Milam et al. 2005), the 12 CO/ 13 CO line ratio indicates that the CO 10–9 emission is optically thick, its optical depth varying between 6.7 ± 1.5 at the peak velocity down to 2.4 ± 0.8 for gas velocities of ~ 5 – 6 km s $^{-1}$ with respect to V_{peak} . Since the 13 CO 10–9 line is optically thin, it can be used to estimate the systemic velocity. The line peak indicates $V_{sys} = +7.7 \pm 0.3$ km s $^{-1}$, consistent with previous estimates from 13 CO and C 18 O 1–0, 2–1 lines (Edwards & Snell 1982; Schuster et al. 1993; Guilloteau et al. 2013).

The [C II] $^2P_{3/2}$ – $^2P_{1/2}$ and SO 12 $_{13}$ –11 $_{12}$ lines peak at slightly blue-shifted velocity with respect to systemic ($V_{peak} = +7.1 \pm 0.2$, $+7.2 \pm 0.5$ km s $^{-1}$). As previously suggested by Guilloteau et al. (2013) SO lines trace the envelope with no evidence of high-velocity wings. The [C II] line instead shows high-velocity blue-shifted and red-shifted wings associated with outflowing gas.

¹⁶ *Herschel* is an ESA space observatory with science instruments provided by European-led Principal Investigator consortia and with important participation from NASA.

¹⁷ HIPE is a joint development by the *Herschel* Science Ground Segment Consortium, consisting of ESA, the NASA *Herschel* Science Center, and the HIFI, PACS, and SPIRE consortia.

¹⁸ <http://www.iram.fr/IRAMFR/GILDAS>

¹⁹ $F_{obs} = (2K_b v^3/c^3) \times \int T_{mb}dV \times \pi(\text{HPBW}/2\sqrt{\ln 2})^2$.

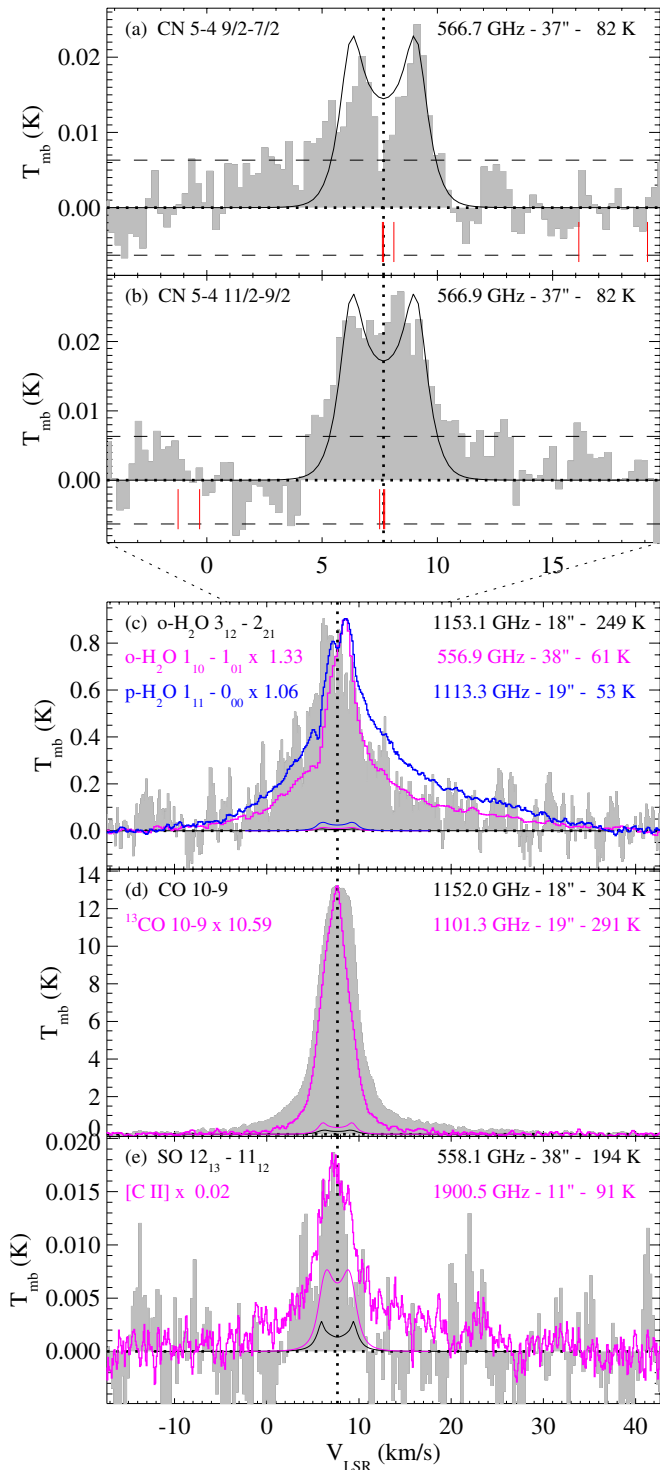


Figure 1. *Herschel*/HIFI spectra of CN 5–4 9/2–7/2 (panel (a)), CN 5–4 11/2–9/2 (panel (b)), o-H₂O 3₁₂–2₂₁, o-H₂O 1₁₀–1₀₁, p-H₂O 1₁₁–0₀₀ (panel (c)), CO 10–9, ¹³CO 10–9 (panel (d)), SO 12₁₃–11₁₂, [C II] ²P_{3/2}–²P_{1/2} (panel (e)). Horizontal and vertical dotted lines indicate the baseline and systemic velocity ($V_{\text{sys}} = +7.7 \text{ km s}^{-1}$). The line frequency, HBPW, and upper level energy are labeled. For CN 5–4 the rms noise is indicated by the dashed horizontal line and the positions of the hyperfine structure lines by the red vertical lines. The line profiles predicted by the ProDiMo disk model of T Tau N are overplotted in black, magenta, and blue (corresponding observed profiles are in gray, magenta, and blue).

(A color version of this figure is available in the online journal.)

We also detect three water lines: the o-H₂O 1₁₀–1₀₁, o-H₂O 3₁₂–2₂₁, and p-H₂O 1₁₁–0₀₀ lines. The two fundamental water lines ($E_{\text{up}} \sim 61, 53 \text{ K}$) show an absorption feature at the systemic velocity, due to the cloud, and a second absorption at $\sim +5.6 \text{ km s}^{-1}$, whose origin is unclear. As already observed in previous works (e.g., Kristensen et al. 2012), water lines appear to be very sensitive to high-velocity emission showing wings extending up to velocities of -12 km s^{-1} and $+40 \text{ km s}^{-1}$.

In contrast with previous observations of CO 6–5, 3–2, 2–1, and 1–0 lines (Edwards & Snell 1982; Schuster et al. 1993), the observed CO 10–9, H₂O, and [C II] lines show a red-shifted wing which is brighter and extends to higher velocities than the blue one. The lines observed with HIFI have higher upper level energies and/or critical densities than previously observed low- J CO lines ($E_{\text{up}} \leq 116 \text{ K}$), thus suggesting that the red-shifted outflowing gas is denser and more excited than the blue-shifted gas.

Our observations also cover the CN $N = 5-4$ hyperfine structure lines²⁰ (Müller et al. 2001). We detect the three brightest $J = 9/2-7/2$ and $J = 11/2-9/2$ lines at 566.7 GHz and 566.9 GHz, while the fainter $J = 9/2-9/2$ components fall outside the observed range. The separation in velocity between the three detected lines is between 0.05 and 0.45 km s^{-1} , and hence the lines are not resolved at the available resolution (0.5 km s^{-1}) and the observed profile is sensitive *only* to the kinematics of the emitting gas. The CN 5–4 $J = 9/2-7/2$ lines show a narrow double-peaked profile centered at the systemic velocity with a total line width of $\sim 7 \text{ km s}^{-1}$, FWHM of $4.0 \pm 0.5 \text{ km s}^{-1}$, and a peak separation $\Delta V_{\text{sep}} = 2.4 \pm 0.5 \text{ km s}^{-1}$. The profile of the $J = 11/2-9/2$ blended components is also narrow and symmetric around the systemic velocity, even though the double-peak is not as clear as in the $J = 9/2-7/2$ lines (see Table 1). The blue-/red-shifted wing shown by the $J = 9/2-7/2$ and the $J = 11/2-9/2$ components, respectively, is clearly due to the noise as it is below the noise level and is not detected in both components. Hence, the CN 5–4 profiles are consistent with emission from the outer region of the disk of T Tau N. The double-peak detected in the CN 5–4 lines is not seen in the 2–1 lines observed with the IRAM 30-m by Guilloteau et al. (2013). This is due to the higher excitation energy and critical density of the CN 5–4 lines ($E_{\text{up}} \sim 82 \text{ K}$, $n_{\text{cr}} \sim 2 \cdot 10^8 \text{ cm}^{-3}$), which makes them less affected by cloud emission, hence more effective to probe the disk, than CN 2–1 ($E_{\text{up}} \sim 16 \text{ K}$, $n_{\text{cr}} \sim 2 \cdot 10^7 \text{ cm}^{-3}$). Emission from the disks of T Tau Sa and T Tau Sb is expected to be negligible with respect to the emission from the disk of T Tau N, as those disks are not detected in the mm continuum and are one to two orders of magnitude less massive and very small (Akeson et al. 1998; Ratzka et al. 2009; Guilloteau et al. 2011).

Assuming Keplerian rotation, a stellar mass of $2.1 M_{\odot}$ and an inclination of $i \simeq 20^{\circ}$ – 30° (Ratzka et al. 2009), the peak separation of the CN lines indicates an outer disk radius $R_{\text{out}}(\text{CN}) < 160\text{--}350 \text{ AU}$. This upper limit is in agreement with the size of the disk as estimated from continuum maps at 1.3, 2.7 mm ($R_{\text{out}}(\text{dust}) = 67 \pm 20 \text{ AU}$, Guilloteau et al. 2011) and from the H₂ ring-like structure observed by Gustafsson et al. (2008) ($R_{\text{out}}(\text{H}_2) = 85\text{--}100 \text{ AU}$).

4. MODELING CN LINES FROM THE DISK OF T Tau N

In order to test if the CN lines originate in the disk of T Tau N we use a parameterized disk model calculated with the

²⁰ Due to the coupling of the rigid-body angular momentum, N , with the electronic spin, S , and with the nuclear spin, I , angular momenta, the CN $N = 5-4$ line is split into 19 hyperfine components characterized by the corresponding quantum numbers $J = N + S$, and $F = J + I$.

Table 2
T Tau N Disk Model: Star and Disk Parameters

Effective temperature	T_{eff} (K)	5250
Stellar mass	M_* (M_{\odot})	2.1
Stellar luminosity	L_* (L_{\odot})	7.3
UV excess	f_{UV}	0.1
UV power law index	p_{UV}	0.2
X-rays luminosity	L_X (erg s^{-1})	$2 \cdot 10^{31}$
Disk inclination	i ($^{\circ}$)	25
Disk inner radius	R_{in} (AU)	0.1
Disk outer radius	R_{out} (AU)	110
Disk dust mass	M_{dust} (M_{\odot})	$1.3 \cdot 10^{-4}$
Dust-to-gas ratio	Dust-to-gas	0.01
Dust material mass density	ρ_{dust} (g cm^{-3})	2.5
Minimum grain size	a_{min} (μm)	0.005
Maximum grain size	a_{max} (μm)	1000
Dust size distribution index	q	3.5
Surface density $\Sigma \approx r^{-\epsilon}$	ϵ	1
Scale height at R_{in}	H_0 (AU)	0.0032
Flaring index $H(r) = H_0 \left(\frac{r}{R_{\text{in}}}\right)^{\beta}$	β	1.25
Settling $H(r, a) = H(r) \frac{a}{a_{\text{set}}}^{-s_{\text{set}}/2}$	s_{set}	0.5
Minimum grain size for settling	a_{set} (μm)	0.25
Fraction of PAHs w.r.t. ISM	f_{PAH}	0.01

thermo-chemical disk modeling code ProDiMo (Woitke et al. 2009; Kamp et al. 2010; Aresu et al. 2011).

We adopt stellar and disk parameters as inferred from previous studies, which well reproduce the source spectral energy distribution (SED; e.g., Ratzka et al. 2009). We use stellar spectral type K0 ($T_{\text{eff}} \simeq 5250$ K), stellar luminosity $\simeq 7.3 L_{\odot}$ and stellar mass $M_* \simeq 2.1 M_{\odot}$ as determined by White & Ghez (2001). The UV spectrum (Calvet et al. 2004) is reproduced by an UV excess $f_{\text{UV}} = L(910\text{--}2500 \text{ \AA})/L_* = 0.1$ and a power law slope $L_{\lambda} \approx \lambda^{0.2}$. The effect of X-ray radiation from the stellar corona of T Tau N ($L_X = 2 \cdot 10^{31} \text{ erg s}^{-1}$; Güdel et al. 2007) is taken into account following Aresu et al. (2011) and Meijerink et al. (2012). Following Ratzka et al. (2009) we assume a disk inner radius $R_{\text{in}} = 0.1$ AU, a dust mixture of astronomical silicates (Draine & Lee 1984) and amorphous carbon (Zubko et al. 1996) with relative abundances of 62.5% and 37.5%, and a grain size distribution $n(a) \approx a^{-q}$ with $q = 3.5$, where $n(a)$ is the number of dust particles with radius a , and the minimum/maximum grain size are $a_{\text{min}} = 0.005 \mu\text{m}$ and $a_{\text{max}} = 1$ mm. This implies a dust mass of $1.3 \cdot 10^{-4} M_{\odot}$ to reproduce the observed mm emission (Hogerheijde et al. 1997; Akeson et al. 1998; Guilloteau et al. 2011). Using the average ISM dust-to-gas ratio of 0.01, the gas mass is $0.013 M_{\odot}$. The dust-to-gas ratio can be different from the ISM value in evolved disks (e.g., Thi et al. 2010; Gorti et al. 2011). However, as the CN lines are optically thick in the disk, their flux is independent on the gas mass, hence on the assumed dust-to-gas ratio. The SED is well reproduced by assuming a disk surface density $\Sigma \approx r^{-1}$ and scale height $H = 0.0032 \text{ AU} (r/R_{\text{in}})^{1.25}$ (Ratzka et al. 2009). To obtain a dust distribution similar to the two-layers model adopted by Ratzka et al. (2009), we assume that grains larger than $a_{\text{set}} = 0.25 \mu\text{m}$ have settled to a smaller scale height than the gas, $H(r, a) = H(r) (a/a_{\text{set}})^{-s_{\text{set}}/2}$, with $s_{\text{set}} = 0.5$. As polycyclic aromatic hydrocarbon (PAH) emission is generally not detected in T Tauri stars (e.g., Furlan et al. 2006), the PAH fraction, f_{PAH} , is set to 0.01 with respect to the ISM abundance of $10^{-6.52}$ PAH particles/H-nucleus. Lower values, $f_{\text{PAH}} = 10^{-3}\text{--}10^{-4}$, do not affect the CN emission. The adopted stellar and disk parameters are summarized in Table 2.

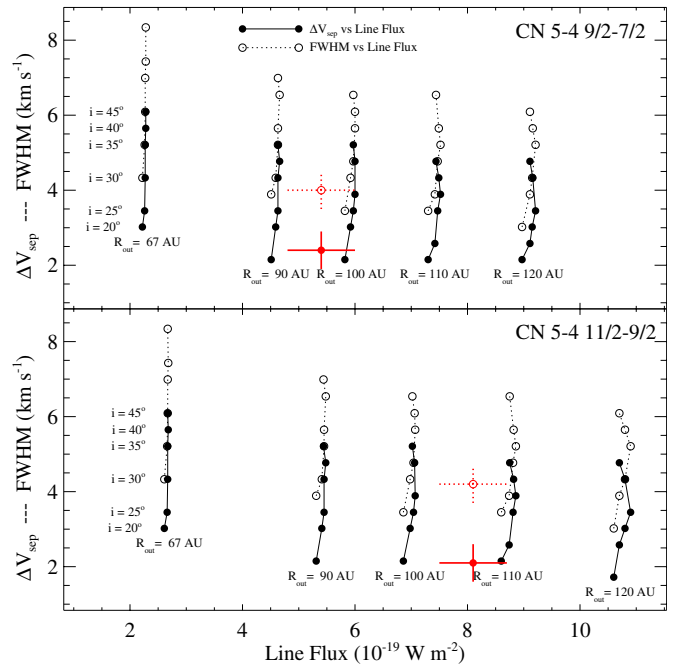


Figure 2. Observed line properties (in red) are compared with model predictions (in black) for different values of the disk outer radius, R_{out} (AU), and inclination, i ($^{\circ}$), for the CN 5-4 $J = 9/2-7/2$ and $J = 11/2-9/2$ lines (top and bottom panel, respectively). The peak separation vs. the line flux is indicated by filled points and solid lines connecting the model predictions for the same R_{out} . The FWHM vs. the line flux is overplotted with empty circles and dotted lines.

(A color version of this figure is available in the online journal.)

As the CN line fluxes and profiles are very sensitive to the assumed disk outer radius, R_{out} , and inclination, i , we proceed through two steps. First, we run a grid of models at low resolution (50×50 grid points) adopting R_{out} and i values which cover the range of estimates from previous studies ($R_{\text{out}} = 67, 90, 100, 110, 120$ AU, $i = 20, 25, 30, 35, 40, 45$ AU; Stapelfeldt et al. 1998; Gustafsson et al. 2008; Ratzka et al. 2009; Guilloteau et al. 2011; Harris et al. 2012). Then, we run a high resolution model (100×100 grid points) for R_{out} and i which best fit the observations, to better resolve the chemical and temperature gradients and the vertical extent of the line forming region in the disk. The predicted FWHM and peak separation do not depend on the model resolution while the line fluxes are lower by up to $\sim 30\%$ when increasing the resolution.

The line profiles and fluxes are obtained by first solving the statistical equilibrium with two-dimensional escape probability to obtain the level populations, and then using two-dimensional ray-tracing. As the three brightest lines of each CN 5-4 $J-J'$ transition are blended and the three undetected components are more than one order of magnitude fainter, the model computes the sum of the CN 5-4 $J = 9/2-7/2$ and $J = 11/2-9/2$ lines. The results obtained for the grid of models (Figure 2) show that the CN line fluxes depend mainly on the disk size and increase for increasing outer radii. This is due to the fact that, as suggested by their profiles, the CN lines originate from the outer region of the disk. The best fit of the CN line fluxes is obtained for $R_{\text{out}} = 100\text{--}110$ AU. However, as model-predicted fluxes are affected by $\sim 30\%$ uncertainty, values of R_{out} between 90 and 120 AU produce CN line fluxes which are still in agreement with the observations. The ratio between the 566.9 and the 566.7 GHz lines predicted by the models, $R_{\text{mod}} = 1.2$, is slightly lower but still in agreement with the observed one ($R_{\text{obs}} = 1.4 \pm 0.2$). The peak separation and

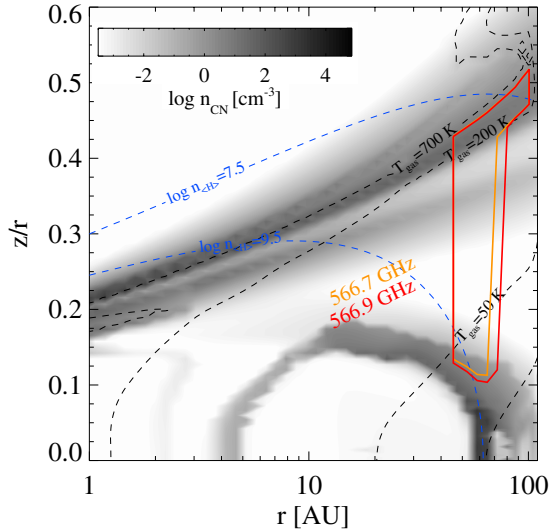


Figure 3. Disk region from which 50% of the CN 5–4 $J = 9/2-7/2$ at 566.7 GHz (in orange), and the CN 5–4 $J = 11/2-9/2$ at 566.9 GHz (in red) line emission arises in the disk model of T Tau N. Note that the emitting regions of the two CN lines overlap almost completely. The gray color indicates the CN density, n_{CN} (cm^{-3}), the dotted black and blue curves the gas temperature and total hydrogen number density $n_{(\text{H})} = n_{\text{H}} + 2n_{\text{H}_2}$.

(A color version of this figure is available in the online journal.)

FWHM predicted by the models depend on both R_{out} and i . For $R_{\text{out}} = 90-120$ AU the observed ΔV_{sep} and FWHM are reproduced if the disk inclination is low ($i = 20^\circ - 30^\circ$). This is in agreement with the conclusions by Akeson et al. (2002) and Ratzka et al. (2009) based on the modeling of the SED and near-, mid-infrared visibilities. Larger inclination angles of $40^\circ-45^\circ$ (Stapelfeldt et al. 1998; Guilloteau et al. 2011) are excluded based on the observed CN profiles.

Following the results obtained from the grid of models, we adopt $R_{\text{out}} = 110$ AU, $i = 25^\circ$ and compute the fluxes and profiles of all the lines covered by our observations using the high resolution model. Figure 3 shows the region in the disk where 50% of the CN $N = 5-4$ $J = 9/2-7/2$ and $J = 11/2-9/2$ lines originate according to our model. This is obtained using vertical escape probability and without accounting for disk inclination. The model indicates that the CN lines are excited in a disk upper layer located at 40–110 AU distance from the star, which is irradiated by the stellar UV field. This heats the gas up to temperatures of $\sim 50-700$ K, while the gas density is $\sim 3 \cdot 10^7-3 \cdot 10^9 \text{ cm}^{-3}$, thus the CN lines are almost thermalized and optically thick ($\tau \sim 10^2-10^3$) in the line emitting region. In this disk layer, CN is produced by $\text{H} + \text{CN}^+$, and $\text{C} + \text{NO}$ reactions, and photo-dissociation of HCN, while the main destruction route is photo-dissociation of CN.

In Figure 1 and Table 1, the model-predicted line profiles and fluxes are compared with the observed ones. For CN lines, the model predicts an FWHM of 3.9 km s^{-1} and peak separation of 2.6 km s^{-1} , in agreement with observations (FWHM = $4.0, 4.2 \pm 0.5 \text{ km s}^{-1}$, $\Delta V_{\text{sep}} = 2.4, 2.1 \pm 0.5 \text{ km s}^{-1}$). Also the line fluxes agree with observations within a factor $\sim 0.9, 1.2$. The sum of the fluxes of the $N = 2-1$ components, instead, is about an order of magnitude lower than what observed by Guilloteau et al. (2013), who suggest that the line is dominated by envelope emission. The CO, ^{13}CO , H_2O , and SO line fluxes predicted by the disk model are from a factor four to two orders of magnitude smaller than observed, as well as for the high- J CO, H_2O , OH, and atomic [O I], [C II] lines previously observed with PACS

(see Table 4 by Podio et al. 2012). This is a further evidence that these lines are dominated by envelope and outflow emission, as already suggested by the fact that [O I], [C II] emission is spatially extended with PACS ($\geq 9''$) and by the broad profiles of CO, H_2O , SO, and [C II] obtained with HIFI.

5. CONCLUSIONS

The *Herschel*/HIFI observations of the T Tau system show emission in a number of molecular and atomic lines. The origin of the emission lines in embedded, accreting/ejecting sources is highly debated, being crucial to identify a tracer to dig out the faint disk emission (e.g., Podio et al. 2012, 2013). In the case of T Tau, the CO, H_2O , and [C II] lines clearly trace high-velocity outflowing gas. By contrast with those lines and with previously observed CN 2–1 lines (Guilloteau et al. 2013), the CN 5–4 lines show narrow double-peaked profiles centered at the systemic velocity, suggesting an origin in the outer disk of T Tau N. Disk modeling predicts CN line fluxes and profiles in agreement with observed ones and constrains the size of the gaseous disk of T Tau N ($R_{\text{out}} = 110_{-20}^{+10}$ AU) and its inclination ($i = 25^\circ \pm 5^\circ$). This study demonstrates that high- J CN lines are a unique tool to probe the gaseous disk of strongly accreting/ejecting sources and paves the way for future observations of embedded disks with ALMA.

L.P. and S.D.B. acknowledge funding from the European FP7 (PIEF-GA-2009-253896) and the National Science Foundation (AST-0954811).

REFERENCES

- Akeson, R. L., Ciardi, D. R., van Belle, G. T., & Creech-Eakman, M. J. 2002, *ApJ*, 566, 1124
- Akeson, R. L., Koerner, D. W., & Jensen, E. L. N. 1998, *ApJ*, 505, 358
- Aresu, G., Kamp, I., Meijerink, R., et al. 2011, *A&A*, 526, A163
- Beckwith, S. V. W., Sargent, A. I., Chini, R. S., & Guesten, R. 1990, *AJ*, 99, 924
- Bohm, K.-H., & Solf, J. 1994, *ApJ*, 430, 277
- Calvet, N., Muzerolle, J., Briceño, C., et al. 2004, *AJ*, 128, 1294
- Chapillon, E., Guilloteau, S., Dutrey, A., Piétu, V., & Guélin, M. 2012, *A&A*, 537, A60
- de Graauw, T., Helmich, F. P., Phillips, T. G., et al. 2010, *A&A*, 518, L6
- Draine, B. T., & Lee, H. M. 1984, *ApJ*, 285, 89
- Duchêne, G., Ghez, A. M., McCabe, C., & Ceccarelli, C. 2005, *ApJ*, 628, 832
- Dutrey, A., Guilloteau, S., & Guélin, M. 1997, *A&A*, 317, L55
- Dutrey, A., Guilloteau, S., Prato, L., et al. 1998, *A&A*, 338, L63
- Edwards, S., & Snell, R. L. 1982, *ApJ*, 261, 151
- Eisloffel, J., & Mundt, R. 1998, *AJ*, 115, 1554
- Furlan, E., Hartmann, L., Calvet, N., et al. 2006, *ApJS*, 165, 568
- Gorti, U., Hollenbach, D., Najita, J., & Pascucci, I. 2011, *ApJ*, 735, 90
- Güdel, M., Telleschi, A., Audard, M., et al. 2007, *A&A*, 468, 515
- Guilloteau, S., Di Folco, E., Dutrey, A., et al. 2013, *A&A*, 549, A92
- Guilloteau, S., Dutrey, A., Piétu, V., & Boehler, Y. 2011, *A&A*, 529, A105
- Gustafsson, M., Labadie, L., Herbst, T. M., & Kasper, M. 2008, *A&A*, 488, 235
- Harris, R. J., Andrews, S. M., Wilner, D. J., & Kraus, A. L. 2012, *ApJ*, 751, 115
- Herbst, T. M., Hartung, M., Kasper, M. E., Leinert, C., & Ratzka, T. 2007, *AJ*, 134, 359
- Hogerheijde, M. R., van Langevelde, H. J., Mundy, L. G., Blake, G. A., & van Dishoeck, E. F. 1997, *ApJL*, 490, L99
- Kamp, I., Tilling, I., Woitke, P., Thi, W.-F., & Hogerheijde, M. 2010, *A&A*, 510, A18
- Köhler, R., Ratzka, T., Herbst, T. M., & Kasper, M. 2008, *A&A*, 482, 929
- Kristensen, L. E., van Dishoeck, E. F., Bergin, E. A., et al. 2012, *A&A*, 542, A8
- Meijerink, R., Aresu, G., Kamp, I., et al. 2012, *A&A*, 547, A68
- Milam, S. N., Savage, C., Brewster, M. A., Ziurys, L. M., & Wyckoff, S. 2005, *ApJ*, 634, 1126
- Müller, H. S. P., Thorwirth, S., Roth, D. A., & Winnewisser, G. 2001, *A&A*, 370, L49
- Öberg, K. I., Qi, C., Fogel, J. K. J., et al. 2010, *ApJ*, 720, 480
- Öberg, K. I., Qi, C., Fogel, J. K. J., et al. 2011, *ApJ*, 734, 98

- Pickett, H. M., Poynter, R. L., Cohen, E. A., et al. 1998, *JQSRT*, **60**, 883
- Piétu, V., Dutrey, A., & Guilloteau, S. 2007, *A&A*, **467**, 163
- Pilbratt, G. L., Riedinger, J. R., Passvogel, T., et al. 2010, *A&A*, **518**, L1
- Podio, L., Kamp, I., Codella, C., et al. 2013, *ApJL*, **766**, L5
- Podio, L., Kamp, I., Flower, D., et al. 2012, *A&A*, **545**, A44
- Qi, C., Ho, P. T. P., Wilner, D. J., et al. 2004, *ApJL*, **616**, L11
- Ratzka, T., Schegerer, A. A., Leinert, C., et al. 2009, *A&A*, **502**, 623
- Roelfsema, P. R., Helmich, F. P., Teyssier, D., et al. 2012, *A&A*, **537**, A17
- Schuster, K. F., Harris, A. I., Anderson, N., & Russell, A. P. G. 1993, *ApJL*, **412**, L67
- Solf, J., & Böhm, K.-H. 1999, *ApJ*, **523**, 709
- Spinoglio, L., Giannini, T., Nisini, B., et al. 2000, *A&A*, **353**, 1055
- Stapelfeldt, K. R., Burrows, C. J., Krist, J. E., et al. 1998, *ApJ*, **508**, 736
- Thi, W.-F., Mathews, G., Ménard, F., et al. 2010, *A&A*, **518**, L125
- Thi, W.-F., van Zadelhoff, G.-J., & van Dishoeck, E. F. 2004, *A&A*, **425**, 955
- van Boekel, R., Güdel, M., Henning, T., Lahuis, F., & Pantin, E. 2009, *A&A*, **497**, 137
- White, R. J., & Ghez, A. M. 2001, *ApJ*, **556**, 265
- Woitke, P., Kamp, I., & Thi, W.-F. 2009, *A&A*, **501**, 383
- Zubko, V. G., Mennella, V., Colangeli, L., & Bussoletti, E. 1996, *MNRAS*, **282**, 1321